

Numerical parametric analysis on the ultimate bearing capacity of the purlin-sheet roofs connected by standing seam clips

Yingying Zhang^{*1}, Xiaoguang Song² and Qilin Zhang³

¹State Key Laboratory for Geomechanics and Deep Underground Engineering, Jiangsu Key Laboratory of Environmental Impact and Structural Safety in Engineering, China University of Mining and Technology, Xuzhou Jiangsu, 221116, China

²Shandong Academy of building research, Jinan Shandong, 250031, China

³College of Civil Engineering, Tongji University, Shanghai, 20092, China

(Received August 2, 2016, Revised March 14, 2017, Accepted March 15, 2017)

Abstract. This paper presents the parametric numerical analysis on the ultimate bearing capacity of the purlin-sheet roofs connected by standing seam clips. The effects of several factors on failure modes and ultimate bearing capacity of the purlins are studied, including setup of anti-sag bar, purlin type, sheet thickness and connection type et al. A simplified design formula is proposed for predicting the ultimate bearing capacity of purlins. Results show that setting the anti-sag bars can improve the ultimate bearing capacity and change the failure modes of *C* purlins significantly. The failure modes and ultimate bearing capacity of *C* purlins are significantly different from those of *Z* purlins, in the purlin-sheet roof connected by standing seam clips. Setting the anti-sag bars near the lower flange is more favorable for increasing the ultimate bearing capacity of purlins. The ultimate bearing capacity of *C* purlins increases slightly with sheet thickness increasing from 0.6 mm to 0.8 mm. The ultimate bearing capacity of the purlin-sheet roofs connected by standing seam clips is always higher than those by self-drilling screws. The predictions of the proposed design formulas are relatively in good agreement with those of EN 1993-1-3: 2006, compared with GB 50018-2002.

Keywords: standing seam clip; purlin-sheet roof; failure mode; ultimate bearing capacity; diaphragm effect

1. Introduction

Cold-formed steel sections are commonly used in a variety of ways such as for purlins, rails, sheeting, decking, storage racking and shelving, etc (Cai *et al.* 2015, 2016). Among these products, purlins and rails are the most common members widely used in buildings. There are three main connection types in the lightweight steel roofs, including self-drilling screws, hidden buckle, and standing seam clips. The sheet-purlin roofs connected by standing seam clips are widely used in recent years. They are popular in practical engineering due to its excellent waterproof sealing performance and corrosion resistance. The standing seam clips and roof sheets are connected by mechanical occlusions, while the bottom of clips and purlins are connected by self-drilling screws (European Committee for Standardization 2003). The slippage of clips may weaken the connection integrity of roof sheets and purlins. The failure modes of sheets connected by clips are different from those connected by self-drilling screws and it is easy to fail under strong wind uplifts.

The air pressure testing is the most effective method to study the ultimate bearing capacity of sheets under wind pressures (Richard 1985). Rousch and Hancock (1997) have ever carried out a series of tests on the sheet-purlin roofs in the University of Sydney, which provide a good reference

for the following researches. Surry *et al.* (2007) carried out the full-size tests to simulate the wind loads on the roof connected by standing seam clips in the Mississippi State University, and found the test results are in good consistent with the tests of the University of Western Ontario. Farquhar *et al.* (2005) conducted the uniform pressure tests and wind tunnel tests on the 1:25 scaled standing seam roofs and discussed the relationship between the static and dynamic ultimate bearing capacities of purlin-sheet roofs. Habte *et al.* (2015) studied the mechanical properties of two types of standing seam roofs (i.e., vertical-leg and trapezoidal) by experiments and found that roof panel profile and perimeter eave attachments can significantly affect uplift pressures and lower deflections are recorded for the vertical-leg roof. The ASCE 7-10 standard was observed to underestimate the corner wind suction on trapezoidal roof. Morrison and Kopp (2012) found that compared with the integrated wind tunnel data, the ASCE 7-05 wind loads for the standing seam clips are conservative, which is primarily due to that the critical clips are not located in the worst aerodynamic region of the roof.

With the development of science and technology, many researchers proposed some improvements on the test methods and design criteria of standing seam roofs (Shoemaker 2009, Prevatt *et al.* 1995). However, due to huge cost and high requirements on the test equipment, most of the researches are carried out by numerical calculations (Cai *et al.* 2012, 2013). Rousch and Hancock (1997) proposed the non-linear elastic analysis method to predict the failure modes and ultimate bearing capacity of

*Corresponding author, Associate Professor
E-mail: zhangyingying85@163.com

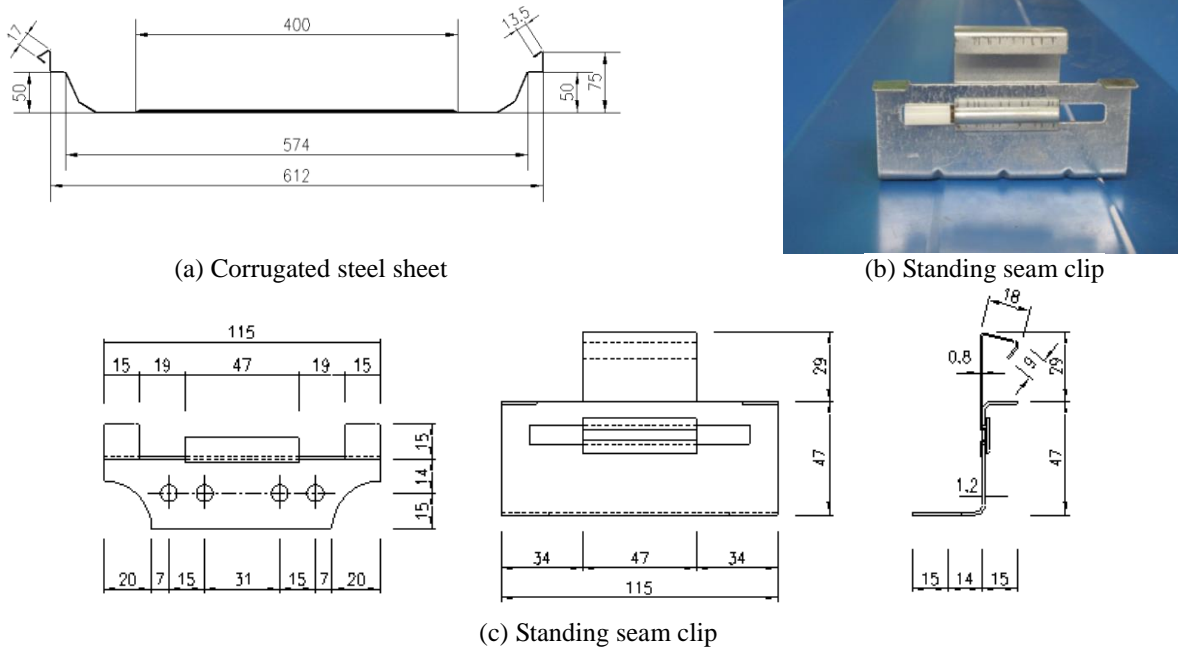


Fig. 1 Dimensions of corrugated steel sheet and standing seam clips

sheet-purlin roof connected by self-drilling screws under wind uplifts. Zhang and Tong (2016) presented two representative buckling theories for the lateral buckling of thin-walled beams and compared with the results of finite element analysis. Ali and Senseny (2003) developed mathematical models to estimate aggregate losses from severe windstorms and developed a three-dimensional static and dynamic analysis approach by using ABAQUS. Mahaarachchi and Mahen (2009) proposed a new shell element to simulate the sheets fixed in the crest, and conducted the parametric studies to obtain the design strength of corrugated steel sheets under wind uplifts.

There are some references on the torsional restraint effect of roof sheets on purlins. Johnston and Hancock (1994) proposed the revisions of the R coefficient method in AISI, regarding to the simple-supported purlins and overlapped continuous purlins. Liu *et al.* (2004) carried out an experiment on 28 groups of profiled corrugated sheets to study the total torsional rigidity provided by the roof sheet, clip and purlin. Kachichian and Dunai (2012) presented the effect of sliding clips and intermediate bridge elements on Z-purlins in standing seam roofs and obtained the lateral stiffness by the test results. El Damatty *et al.* (2003) put forward a finite element method to simulate the sheets connected by standing seam clips and found that the relative displacement of sheets in the vertical occlusions determined the failure of clips connection. Katnam *et al.* (2007) proposed a nonlinear finite element model to assess the restraints of sheets on the torsion deformations of purlins. Vrani (2006) thought that the restraints of sheets on the Z and C purlins are affected by external loadings and proposed the corresponding design formula. Lucas *et al.* (1997) proposed two nonlinear elastic-plastic models for the analysis of purlin-sheet roofs. Schafer and Pekoz (1999) proposed the method to analyze the local buckling and the

distortional buckling of the cold-formed flexural members with flange stiffeners. Serrette and Pekoz (1997) proposed the theoretical formulas for the elastic distortional buckling of standing seam roofs by considering both local buckling and distortional buckling.

This paper presents the parametric numerical analysis on the ultimate bearing capacity of the purlin-sheet roof connected by standing seam clips. First, the numerical analysis method is verified by the experiment data in current references. Then, the effects of several factors on the failure modes and ultimate bearing capacity of the purlins are studied, including anti-sag bars, purlin type, sheet thickness and connection type *et al.* Finally, the simplified design formulas are proposed and compared with the current design codes.

2. Materials and methodology

The typical two-span roofs shown in Reference 23 (Song 2012) are taken as the research object. The corrugated steel sheet is HV-612 with the thickness of 0.6 mm. The corrugated steel sheets are made by Q345 and the purlin is made by Q235. The dimensions of corrugated steel sheets and standing seam clips are shown in Fig. 1. According to different cross sections, the purlin spans are 6.0 m, 7.5 m and 9.0 m, respectively. In order to ensure reliability of mechanical occlusion, the thickness of the corrugated steel sheet is generally not less than 0.6 mm. Therefore, 0.6 mm and 0.8 mm are considered in this analysis. Three types of referenced specimens are studied, including without anti-sag bars, one row of bars and two rows of bars, named as “C-0, C-1 and C-2”. As two typical cross sections, the mechanical mechanisms and failure modes of C purlins and Z purlins are also compared in this

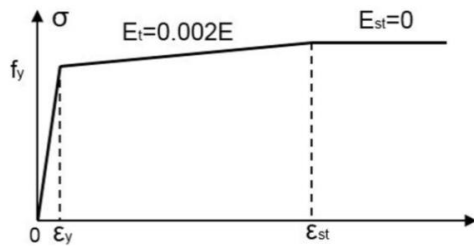


Fig. 2 Stress-strain curves of standing seam clips

analysis. Besides, as two typical connection methods in practical engineering, the self-drilling screw connection and standing seam clips connection are also compared.

In the numerical analysis, the shell element (SHELL 181) is used to simulate the purlins, clips and corrugated steel sheets, while the link element (LINK 8) is used to simulate the anti-sag bars. In order to simulate the contact behaviors of purlins and sheets, the target element (TARGET 170) and contact element (CONTACT 173) is conducted. The sheet surface is defined as the contact surface, while the purlin surface is defined as the target surface. Considering different failure modes of components, the classical elastoplastic model is used for purlins and corrugated steel sheets, while the tri-linear elastoplastic model is used for standing seam clips. The details can be seen in Fig. 2. Where, ε_y is 0.17%, $\varepsilon_{st}=12 \varepsilon_y=2.04\%$, and f_u is 420 MPa. The wind suctions are simulated by uniform pressure applied on the sheet surface.

The boundary conditions of standing seam clips and purlins are defined as follows. Considering that the self-drilling screws are fixed tightly, the slippage does not appear in the tests, so the displacement of clips base and purlin flange are coupled. Besides, from the previous wind suction tests, the support adjustment of standing seam clips is tightly connected with the upper part of the base, therefore, the corresponding displacements of the adjustment and the base are coupled. Considering the adjustment can slide in the groove of the base, the translational displacement U_z of the two parts are not coupled. Besides, the connections of standing seam clips and adjacent corrugated steel sheets are coupled.

3. Results and discussions

3.1 Verification of numerical models

The numerical analysis is carried out to validate the full-size experiment shown in the reference (Song 2012). The section of the purlin is C180×2.5 made by Q345. The dimensions of standing seam clips are shown in Fig. 1. The thickness of the base sheet is 0.64 mm with the yield strength of 427 MPa. The thicknesses of the base and the adjustment are 1.4 mm and 0.8 mm, respectively. The slippage failure appears in the clips between the middle sheet and adjacent purlin. Significant torsional deformations can be observed in the connection between the upper part of the standing seam clip and the adjustment. Here, the maximum stress is 390 N/mm², which has exceeded the

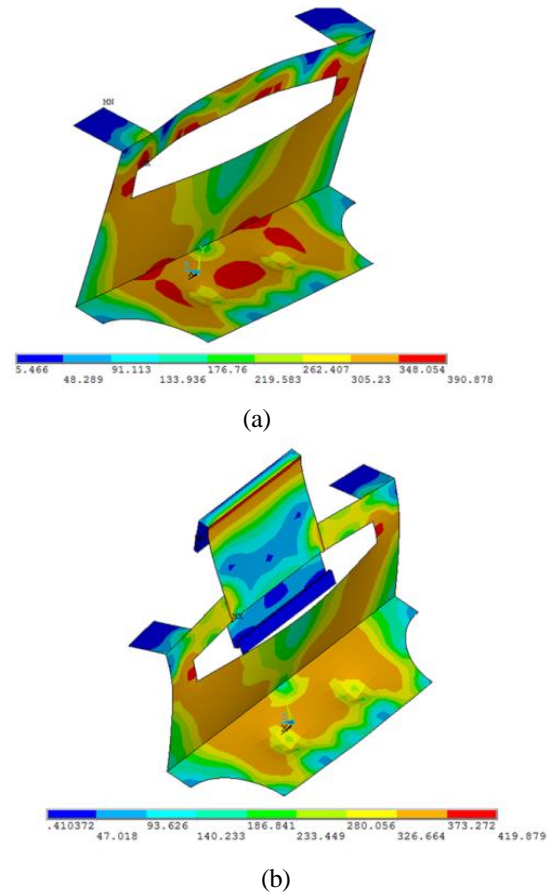


Fig. 3 Failure modes of standing seam clips

Table 1 Comparisons between the test results and the numerical calculation

	Full-size experiment	Numerical calculation
Uniform Pressure P_u (kPa)	1.98	2.13
Ultimate bearing capacity of standing clips T_u (kN)	1.82	1.96
Failure position	Standing clips	Standing seam clips
Failure modes	The base of the standing clip is tensioned fracture, significant distortional deformation in the conjunction of base and adjustment, the adjustment is pulled out from the base	The base of the standing clips is in the elastoplastic phase, significant distortional deformation of the conjunction of the base and the adjustment, the adjustment is pulled out from the base

yield strength, as shown in Fig. 3(a). The adjustment is pulled out from the clip base, as shown in Fig. 3(b).

The comparisons between test results and numerical simulations are shown in Table 1. It can be seen that the deviations between numerical simulations and test results are approximately 7%. The failure load of standing seam clips is 1.96kN, which can be calculated according to the

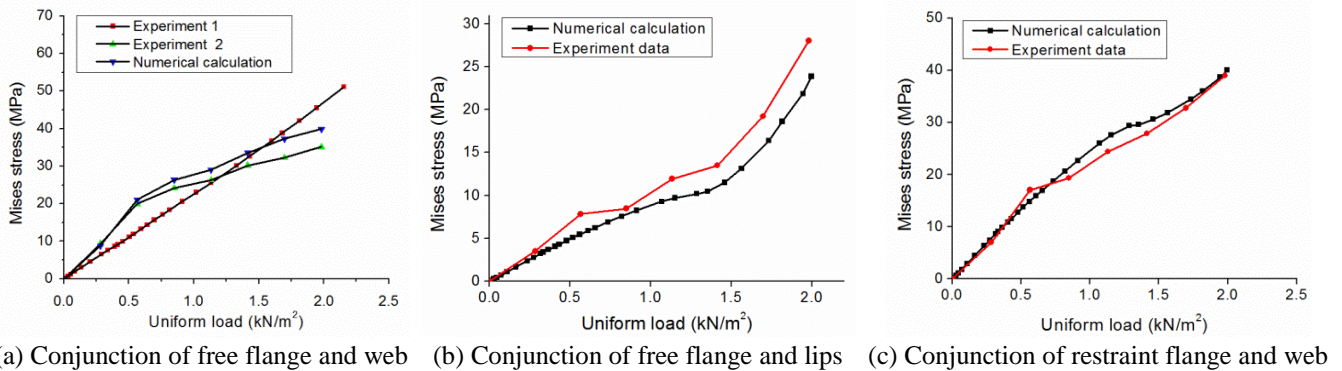


Fig. 4 Comparisons of load-stress curves of the mid-span section of purlins

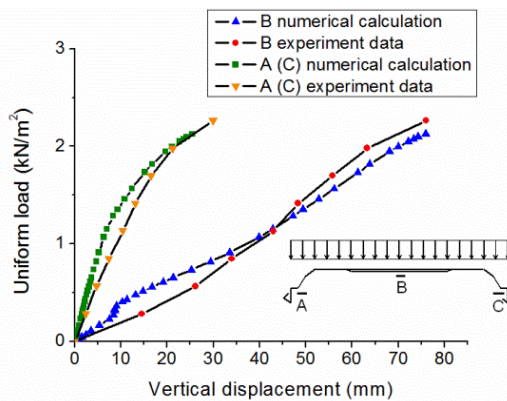


Fig. 5 Comparisons of load-deflection curves of the mid-span section of corrugated steel sheet

subordinate area of standing seam clips. The load-stress curves of three parts are listed in Table 4, including the conjunction of free flange and web, the conjunction of free flange and lips, and the conjunction of restraint flange and web. Table 4 shows that the numerical calculation agrees well with the test results. In the initial, the numerical structural stiffness is slightly higher than the measured data. In the ultimate phase, the degradation of the numerical stiffness is more obvious, while the measured data is almost linear. This is because that the numerical model may not accurately reflect initial imperfections and possible errors in the manufacture process.

The vertical displacement-load curves of the middle part (B point) and the stiffening rib on the corrugated steel sheet (at A and C points) are shown in Fig. 5. It can be seen that the numerical calculations are consistent with the test results. From above, the calculated ultimate bearing capacity and failure modes are in good agreement with the measured data. However, there are still some slightly differences between them, which may be related with the initial imperfections of the specimen, the processing and assembling process and the application of uniform loadings. Therefore, the numerical analysis method is reliable and can be used for the parametric analysis.

3.2 Referenced specimens

Table 2 shows the numerical calculations of ultimate bearing capacity of referenced specimens. Where, the

ultimate moment M_{uN} is obtained by the model of simple-supported beam. The yield moment M_y is obtained according to the edge yield of cross section. The factor ϕ_1 is the ratio of ultimate moment M_{uN} on the yield moment M_y . The resistance coefficient γ_R is 1.09 for Q235 (GB 50017, 2003). For the referenced specimens in Table 2, the anti-sag bars are set in 1/3 height of beam web.

As show in Table 2, with span increasing, the ultimate linear load decreases, but the ultimate moment increases. For example, for C160×2.0-6.0, the ultimate linear load of C-0 purlin is 0.95 kN/m and the ultimate moment is 4.28 kN·m. For C160×2.0-7.5, the ultimate linear load of C-0 purlin is 0.73 and the corresponding ultimate moment is 5.13 kN·m. This is mainly related with the restraints of corrugated steel sheet and anti-sag bars. Generally, for traditional beam components, the ultimate bearing capacity decreases with purlin span increasing. However, in this test, the increasing of purlin span also means increasing of restraints provided by corrugated steel sheets. As we know, the diaphragm effect of corrugated steel sheet is very important in the purlin-sheet roof connected by standing seam clips. Therefore, with purlin span increasing, the ultimate flexural capacity of purlins increases, which is different from the traditional beam components.

3.3 Comparisons between C purlins and Z purlins

For C-0 purlin, the failure mode is the overall buckling of lower flange, as shown in Fig. 6(a), whereas the stress at the junction of the web/lower flange in the middle span achieves the yield strength. For C-1, the failure mode is distortional buckling of lower flange in the middle span where the anti-sag bars are set, as shown in Fig. 6(b). For C-2, the main failure modes are overall buckling of the lower flange at the 1/3 points where the anti-sag bars are set, while the stress in the junction of the web/lower flange achieve the yield strength, as shown in Fig. 6(c).

From Fig. 6, the failure modes of C-section and Z-section purlin are significantly different. For C-0 and Z-0, large lateral displacement and significant torsion can be observed. The failure modes are overall buckling of the lower flange and the junction of the web/lower flange in the middle span achieves the yield strength. The failure mode of C-1 and Z-1 are similar and their failure modes are distortional buckling of the lower flange in the middle span.

Table 2 Numerical calculations of referenced specimens

Purlin type-span	C-0			C-1			C-2		
	M_{uN} (kN·m)	$\varphi_1 = \frac{M_{uN}}{M_y}$	$\varphi = \frac{\varphi_1}{\gamma_R}$	M_{uN} (kN·m)	$\varphi_1 = \frac{M_{uN}}{M_y}$	$\varphi = \frac{\varphi_1}{\gamma_R}$	M_{uN} (kN·m)	$\varphi_1 = \frac{M_{uN}}{M_y}$	$\varphi = \frac{\varphi_1}{\gamma_R}$
C140×2.0-6.0	3.51	0.68	0.62	4.82	0.93	0.85	4.68	0.91	0.83
C140×2.2-6.0	4.01	0.71	0.65	5.40	0.96	0.88	5.31	0.95	0.87
C140×2.5-6.0	4.82	0.77	0.70	6.26	1.00	0.92	6.57	1.05	0.96
C160×2.0-6.0	4.28	0.62	0.56	6.21	0.89	0.82	6.35	0.91	0.84
C160×2.2-6.0	4.86	0.64	0.59	7.07	0.93	0.86	7.07	0.93	0.86
C160×2.5-6.0	5.85	0.69	0.63	8.28	0.98	0.90	8.15	0.96	0.88
C180×2.0-6.0	5.18	0.58	0.53	7.43	0.83	0.76	8.46	0.94	0.86
C180×2.2-6.0	5.94	0.61	0.56	8.51	0.87	0.80	9.00	0.92	0.84
C180×2.5-6.0	7.07	0.64	0.59	9.05	0.82	0.76*	9.14	0.83	0.76*
C200×2.0-6.0	5.40	0.52	0.48	8.19	0.79	0.73	9.05	0.87	0.80*
C200×2.2-6.0	6.35	0.56	0.52	9.09	0.81	0.74*	9.14	0.81	0.74*
C200×2.5-6.0	7.56	0.60	0.55	9.23	0.73	0.67*	9.23	0.73	0.67*
C160×2.0-7.5	5.13	0.67	0.68	6.05	0.87	0.80	6.12	0.88	0.81
C160×2.2-7.5	5.27	0.70	0.64	6.82	0.90	0.83	6.89	0.91	0.84
C160×2.5-7.5	6.40	0.76	0.69	8.02	0.95	0.87	8.09	0.96	0.88
C180×2.0-7.5	5.48	0.61	0.56	7.95	0.88	0.81	8.02	0.89	0.82
C180×2.2-7.5	6.26	0.64	0.59	8.86	0.90	0.83	9.00	0.92	0.84
C180×2.5-7.5	7.45	0.68	0.62	10.20	0.93	0.85	10.41	0.95	0.87
C200×2.0-7.5	5.77	0.56	0.51	8.93	0.86	0.79	9.07	0.88	0.80
C200×2.2-7.5	6.61	0.59	0.54	9.91	0.88	0.81	10.27	0.91	0.84
C200×2.5-7.5	7.95	0.63	0.58	11.32	0.90	0.82	11.88	0.94	0.86
C220×2.0-7.5	6.33	0.52	0.47	9.70	0.79	0.73	10.62	0.87	0.79
C220×2.2-7.5	7.38	0.55	0.51	10.83	0.81	0.74	12.23	0.91	0.84
C220×2.5-7.5	8.86	0.59	0.54	13.57	0.90	0.83	14.41	0.96	0.88*
C250×2.0-7.5	6.75	0.47	0.43	10.97	0.76	0.69	12.80	0.88	0.81
C250×2.2-7.5	7.88	0.50	0.46	12.23	0.77	0.71	14.20	0.89	0.82*
C250×2.5-7.5	9.49	0.53	0.49	14.13	0.79	0.72*	14.13	0.79	0.72*
C220×2.0-9.0	6.68	0.54	0.50	9.92	0.81	0.74	10.23	0.83	0.76
C220×2.2-9.0	7.80	0.58	0.53	10.94	0.82	0.75	11.64	0.87	0.80
C220×2.5-9.0	9.32	0.62	0.57	12.76	0.85	0.78	13.67	0.91	0.83
C250×2.0-9.0	6.99	0.48	0.44	11.34	0.82	0.72	11.64	0.80	0.74
C250×2.2-9.0	8.20	0.52	0.47	12.45	0.78	0.72	13.47	0.85	0.78
C250×2.5-9.0	9.92	0.55	0.51	14.28	0.80	0.73	15.90	0.89	0.81
C280×2.5-9.0	10.13	0.46	0.43	15.90	0.73	0.67	18.02	0.83	0.76
C280×3.0-9.0	13.47	0.52	0.48	20.05	0.77	0.71	20.66	0.80	0.73*
C300×2.5-9.0	11.24	0.45	0.41	18.83	0.76	0.69	20.86	0.84	0.77*
C300×3.0-9.0	14.68	0.50	0.45	20.45	0.69	0.63*	20.86	0.70	0.65*

For C-2 purlin, the failure mode is overall buckling of the purlins at where the anti-sag bars are set, and the compressive stress at the conjunction of the web/lower flange in the middle span can achieve the yield strength. Meanwhile, for Z-2 purlin, the failure mode is distortional buckling of cross sections between the anti-sag bars, and the compressive stress at the conjunction of the web and lower flange in the middle span can achieve the yield strength.

Besides, there are significant differences between the ultimate bearing capacities of C purlins and Z purlins, as shown in Table 3. Compared with C-0, the maximum, minimum and average increase of Z-0 purlins is 37.00%,

2.74% and 21.13%, respectively. However, the ultimate bearing capacity of Z-1 purlins is lower than that of C-1 purlins. For C-1, the maximum, minimum and average decrease of the ultimate bearing capacity is 26.19%, 2.44% and 18.92%, respectively. For most of Z-2 purlins, the corresponding ultimate bearing capacities are lower than those of C-2 purlins, while the rest are higher than C-2. The maximum increase, maximum decrease and average decrease are 3.38%, 18.68% and 7.32%, respectively. The differences between them are mainly related with the deformation mechanisms of Z purlins and C purlins, as shown in Fig. 6 and Fig. 7. Fig. 7(c) and (d) shows the

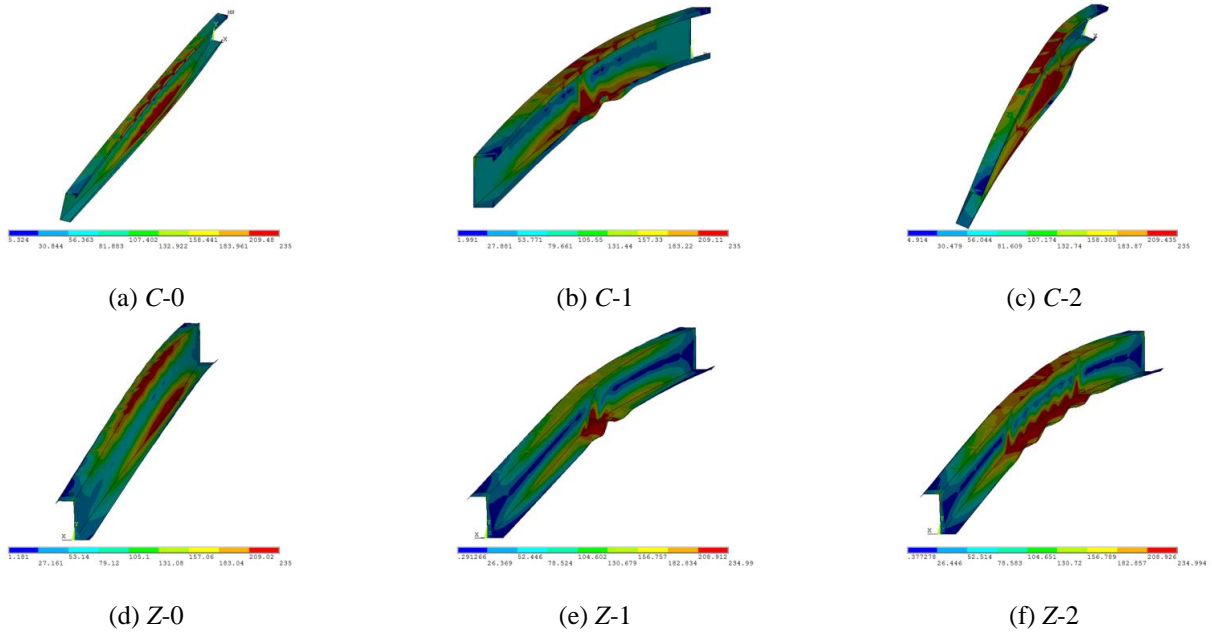


Fig. 6 Failure modes of C purlins and Z purlins

Table 3 Comparisons between the numerical analysis results of C purlins and Z purlins (kN/m)

Purlin type-span	C-0		C-1		C-2	
	q_{uNC}	q_{uNZ}	q_{uNC}	q_{uNZ}	q_{uNC}	q_{uNZ}
140×2.0-6	0.78	0.87	1.07	0.88	1.04	1.02
140×2.2-6	0.89	0.99	1.20	1.00	1.18	1.16
140×2.5-6	1.07	1.17	1.39	1.15	1.46	1.39
160×2.0-6	0.95	1.09	1.38	1.10	1.41	1.31
160×2.2-6	1.08	1.24	1.57	1.26	1.57	1.51
160×2.5-6	1.30	1.46	1.84	1.51	1.81	1.68
180×2.0-6	1.15	1.36	1.65	1.41	1.88	1.65
180×2.2-6	1.32	1.54	1.89	1.55	2.00	1.85
180×2.5-6	1.57	1.81	2.01	1.85	2.03	2.01
200×2.0-6	1.20	1.53	1.82	1.50	2.01	1.82
200×2.2-6	1.41	1.83	2.02	1.76	2.03	2.03
200×2.5-6	1.68	2.00	2.05	2.00	2.05	2.02
160×2.0-7.5	0.73	0.75	0.86	0.68	0.87	0.82
160×2.2-7.5	0.75	0.85	0.97	0.77	0.98	0.94
160×2.5-7.5	0.91	0.98	1.14	0.94	1.15	1.11
180×2.0-7.5	0.78	0.89	1.13	0.85	1.14	1.05
180×2.2-7.5	0.89	1.02	1.26	0.93	1.28	1.21
180×2.5-7.5	1.06	1.21	1.45	1.17	1.48	1.53
200×2.0-7.5	0.82	1.00	1.27	0.97	1.29	1.14
200×2.2-7.5	0.94	1.14	1.41	1.07	1.46	1.32
200×2.5-7.5	1.13	1.34	1.61	1.25	1.69	1.62
220×2.0-7.5	0.90	1.13	1.38	1.10	1.51	1.30
220×2.2-7.5	1.05	1.30	1.54	1.25	1.74	1.46
220×2.5-7.5	1.26	1.54	1.93	1.47	2.05	1.76
250×2.0-7.5	0.96	1.27	1.56	1.29	1.82	1.48
250×2.2-7.5	1.12	1.46	1.74	1.45	2.02	1.65
250×2.5-7.5	1.35	1.74	2.01	1.71	2.01	1.97
220×2.0-9.0	0.66	0.81	0.98	0.73	1.01	0.91
220×2.2-9.0	0.77	0.93	1.08	0.82	1.15	1.06
220×2.5-9.0	0.92	1.11	1.26	0.97	1.35	1.38
250×2.0-9.0	0.69	0.90	1.12	0.85	1.15	1.01
250×2.2-9.0	0.81	1.04	1.23	0.96	1.33	1.17
250×2.5-9.0	0.98	1.25	1.41	1.12	1.57	1.53
280×2.5-9.0	1.00	1.37	1.57	1.29	1.78	1.62
280×3.0-9.0	1.33	1.77	1.98	1.62	2.04	1.82
300×2.5-9.0	1.11	1.50	1.86	1.46	2.06	1.71
300×3.0-9.0	1.45	1.94	2.02	1.84	2.06	2.02

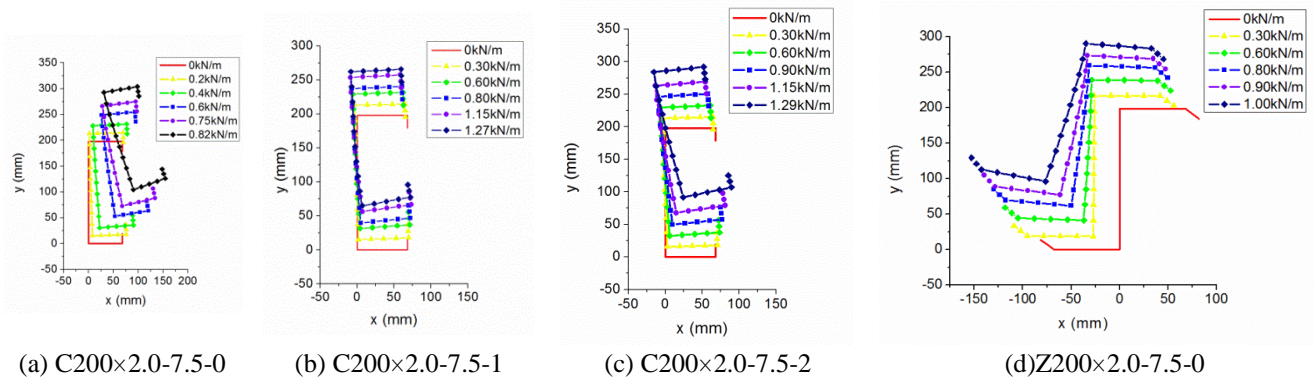


Fig. 7 Variations of purlins during the loading process

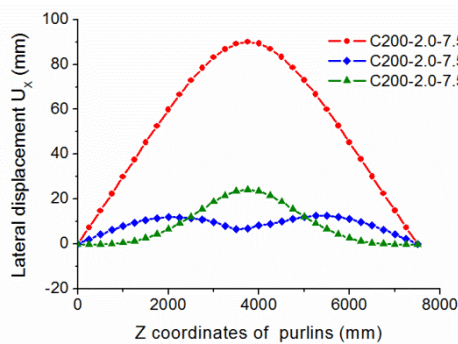


Fig. 8 Lateral displacement of C purlins

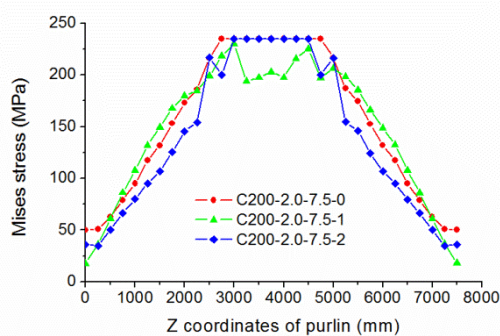


Fig. 9 Stress variations of C purlins

variations of cross section in the middle span for two types of specimens. It can be seen that under the same loading condition, the lateral displacement and torsional displacement of Z purlins are significantly lower than C-purlins. It is easier for Z purlins to achieve its ultimate flexural capacity.

3.4 Number and position of anti-sag bars

Fig. 8 shows the ultimate lateral displacement of web/flange junction of purlins along the span, when the specimens achieve the ultimate bearing capacity. Table 4 shows the effect of setting anti-sag bars on the ultimate bearing capacity of C purlins. Compared with C-0, the maximum, minimum and average increase of the ultimate bearing capacity of C-1 is 67.57%, 17.81% and 43.92%, respectively. Compared with C-1, the maximum increase of the ultimate bearing capacity of C-2 is about 16.67%, the

Table 4 Effect of number and position of anti-sag bars on the ultimate bearing capacity of C purlins

Purlin type-span	Ultimate bearing capacity q_{uN} (kN/m)			$q_{uN1} - q_{uN0}$	$q_{uN2} - q_{uN1}$
	Without	One row	Two rows		
	q_{uN0}	q_{uN1}	q_{uN2}	q_{uN0}	q_{uN1}
C140x2.0-6	0.78	1.07	1.04	37.18%	-2.80%
C140x2.2-6	0.89	1.20	1.18	34.83%	-1.67%
C140x2.5-6	1.07	1.39	1.46	29.91%	5.04%
C160x2.0-6	0.95	1.38	1.41	45.26%	2.17%
C160x2.2-6	1.08	1.57	1.57	45.37%	0.00%
C160x2.5-6	1.30	1.84	1.81	41.54%	-1.63%
C180x2.0-6	1.15	1.65	1.88	43.48%	13.94%
C180x2.2-6	1.32	1.89	2.00	43.18%	5.82%
C180x2.5-6	1.57	2.01	2.03	28.03%	1.00%
C200x2.0-6	1.20	1.82	2.01	51.67%	10.44%
C200x2.2-6	1.41	2.02	2.03	43.26%	0.50%
C200x2.5-6	1.68	2.05	2.05	22.02%	0.00%
C160x2.0-7.5	0.73	0.86	0.87	17.81%	1.16%
C160x2.2-7.5	0.75	0.97	0.98	29.33%	1.03%
C160x2.5-7.5	0.91	1.14	1.15	25.27%	0.88%
C180x2.0-7.5	0.78	1.13	1.14	44.87%	0.88%
C180x2.2-7.5	0.89	1.26	1.28	41.57%	1.59%
C180x2.5-7.5	1.06	1.45	1.48	36.79%	2.07%
C200x2.0-7.5	0.82	1.27	1.29	54.88%	1.57%
C200x2.2-7.5	0.94	1.41	1.46	50.00%	3.55%
C200x2.5-7.5	1.13	1.61	1.69	42.48%	4.97%
C220x2.0-7.5	0.90	1.38	1.51	53.33%	9.42%
C220x2.2-7.5	1.05	1.54	1.74	46.67%	12.99%
C220x2.5-7.5	1.26	1.93	2.05	53.17%	6.22%
C250x2.0-7.5	0.96	1.56	1.82	62.50%	16.67%
C250x2.2-7.5	1.12	1.74	2.02	55.36%	16.09%
C250x2.5-7.5	1.35	2.01	2.01	48.89%	0.00%
C220x2.0-9	0.66	0.98	1.01	48.48%	3.06%
C220x2.2-9	0.77	1.08	1.15	40.26%	6.48%
C220x2.5-9	0.92	1.26	1.35	36.96%	7.14%
C250x2.0-9	0.69	1.12	1.15	62.32%	2.68%
C250x2.2-9	0.81	1.23	1.33	51.85%	8.13%
C250x2.5-9	0.98	1.41	1.57	43.88%	11.35%
C280x2.5-9	1.00	1.57	1.78	57.00%	13.38%
C280x3.0-9	1.33	1.98	2.04	48.87%	3.03%
C300x2.5-9	1.11	1.86	2.06	67.57%	10.75%
C300x3.0-9	1.45	2.02	2.06	39.31%	1.98%

Table 5 Effect of the position of the anti-sag bars on the ultimate bearing capacity of C purlins

Purlin type - span	Ultimate capacity (kN/m)			Ultimate capacity (kN/m)		
	q_{uNb}	q_{uNm}	$\frac{q_{uNm} - q_{uNb}}{q_{uNb}}$	q_{uNb}	q_{uNm}	$\frac{q_{uNm} - q_{uNb}}{q_{uNb}}$
			q_{uNb}			q_{uNb}
C140×2.0-6-1	1.07	1.10	2.80%	1.04	1.00	-3.85%
C160×2.0-6-1	1.38	1.36	-1.45%	1.41	1.29	-8.51%
C180×2.0-6-1	1.65	1.52	-7.88%	1.88	1.54	-18.09%
C200×2.0-6-1	1.82	1.55	-14.84%	2.01	1.66	-17.41%
C160×2.0-7.5-1	0.86	0.91	5.81%	0.87	0.82	-5.75%
C180×2.0-7.5-1	1.13	1.10	-2.65%	1.14	1.00	-12.28%
C200×2.0-7.5-1	1.27	1.24	-2.36%	1.29	1.12	-13.18%
C220×2.0-7.5-1	1.38	1.36	-1.45%	1.51	1.37	-9.27%
C250×2.0-7.5-1	1.56	1.42	-8.97%	1.82	1.45	-20.33%
C220×2.0-9-1	0.98	1.04	6.12%	1.01	0.93	-7.92%
C250×2.0-9-1	1.12	1.17	4.46%	1.15	1.05	-8.70%
C280×3.0-9-1	1.98	1.98	0.00%	2.04	2.00	-1.96%
C300×3.0-9-1	2.02	2.00	-0.99%	2.06	2.00	-2.91%

Table 6 Effect of sheet thickness on the ultimate bearing capacity of C purlins (kN/m)

Purlin type-span	C-0		C-1		C-2	
	$q_{uN0.6}$	$q_{uN0.8}$	$q_{uN0.6}$	$q_{uN0.8}$	$q_{uN0.6}$	$q_{uN0.8}$
C140×2.0-6-0	0.78	0.79	1.07	1.07	1.04	1.05
C160×2.0-6-0	0.95	0.96	1.38	1.38	1.41	1.41
C180×2.0-6-0	1.15	1.17	1.65	1.66	1.88	1.89
C200×2.0-6-0	1.20	1.24	1.82	1.84	2.01	2.04
C160×2.0-7.5-0	0.73	0.73	0.86	0.87	0.87	0.88
C180×2.0-7.5-0	0.78	0.79	1.13	1.13	1.14	1.14
C200×2.0-7.5-0	0.82	0.83	1.27	1.26	1.29	1.29
C220×2.0-7.5-0	0.90	0.91	1.38	1.38	1.51	1.61
C250×2.0-7.5-0	0.96	0.96	1.56	1.56	1.82	1.78
C220×2.0-9-0	0.66	0.67	0.98	0.98	1.01	1.02
C250×2.0-9-0	0.69	0.70	1.12	1.16	1.15	1.16
C280×2.5-9-0	1.00	1.04	1.57	1.58	1.78	1.78
C300×2.5-9-0	1.11	1.14	1.86	1.86	2.06	2.06

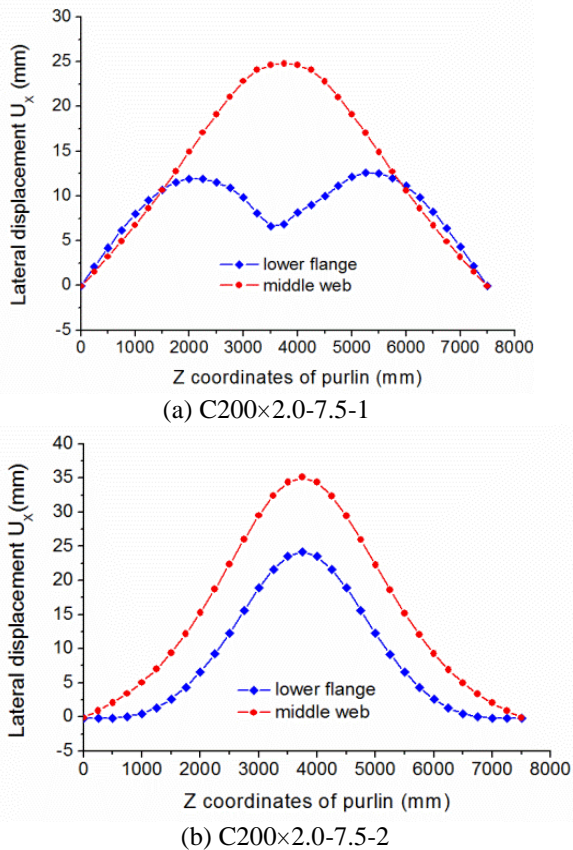


Fig. 10 Effect of position of anti-sag bars on the lateral displacement of purlins

maximum decrease is about 2.80% and the average increase is about 4.86%. After setting the anti-sag bars, the lateral displacement and torsion deformation of C purlins have been restrained significantly and the ultimate flexural capacity increased greatly.

Fig. 9 shows the stress variations at the web/lower flange junction along the span when the specimens achieve

the ultimate bearing capacity. The stress distribution of C-0 purlin is more uniform and a large area can achieve the yield strength. The stress of C-1 is a little lower than the yield strength and the failure mode is elastic distortional buckling, so the ultimate bearing capacity is lower than C-0. For C-2, the stress can achieve the yield strength and the failure mode is elastoplastic distortional buckling.

Fig. 10 shows that the lateral displacement of the web/lower flange junction along the span, C200×2.0-7.5-1, and C200×2.0-7.5-2. Table 5 shows the effects of the position of anti-sag bars on ultimate bearing capacity of C purlins. Where, q_{uNb} is the ultimate bearing capacity when the anti-sag bars are set in the 1/3 height of the web and q_{uNm} is when the anti-sag bars are set in the 1/3 height of the web. The ultimate bearing capacities of C purlins whose anti-sag bars are set in the middle of the web are lower than those whose anti-sag bars are set near the bottom flange. For C-1 purlins, the maximum and average decrease is 14.84% and 1.65%, respectively. For C-2, the maximum, minimum and average decreases are 20.33%, 1.96% and 10.01%, respectively. From above, setting the anti-sag bars near the lower flange is more effective for restraining the lateral displacement and increasing the ultimate bearing capacities of purlins.

3.5 Thickness of corrugated steel sheet

Table 6 shows the effect of sheet thickness on the ultimate bearing capacity of C purlins. Where, $q_{uN0.6}$ and $q_{uN0.8}$ are the ultimate bearing capacity of C purlins whose thickness is 0.6 mm and 0.8 mm, respectively. The ultimate bearing capacity of C purlins increased slightly with sheet thickness increasing from 0.6 mm to 0.8 mm. The main reason is that the roof and the purlins are connected by standing seam clips, not by self-drilling screws. This connection can slide, which can weaken the restraints of the roof on the purlins. The distance of standing clips is always 2-3 times than that of self-drilling screws, which also weakens the integrity of connections between corrugated steel sheets and purlins. It should be noted that the thickness

Table 7 Comparisons of the numerical analysis results of C purlins (kN/m)

Purlin type-span	C-0		C-1		C-2	
	q_{uND}	q_{uNS}	q_{uND}	q_{uNS}	q_{uND}	q_{uNS}
C140×2.0-6	0.85	0.78	1.03	1.07	1.13	1.04
C140×2.2-6	0.92	0.89	1.18	1.20	1.25	1.18
C140×2.5-6	1.04	1.07	1.36	1.39	1.43	1.46
C160×2.0-6	1.07	0.95	1.29	1.38	1.52	1.41
C160×2.2-6	1.19	1.08	1.44	1.57	1.69	1.57
C160×2.5-6	1.33	1.30	1.70	1.84	1.94	1.81
C180×2.0-6	1.29	1.15	1.50	1.65	1.93	1.88
C180×2.2-6	1.45	1.32	1.68	1.89	2.10	2.00
C180×2.5-6	1.66	1.57	2.00	2.01*	2.44	2.03
C200×2.0-6	1.36	1.20	1.65	1.82	2.11	2.01
C200×2.2-6	1.54	1.41	1.94	2.02*	2.37	2.03
C200×2.5-6	1.77	1.68	2.31	2.05*	2.77	2.05
C160×2.0-7.5	0.72	0.73	0.84	0.86	0.93	0.87
C160×2.2-7.5	0.78	0.75	0.95	0.97	1.04	0.98
C160×2.5-7.5	0.88	0.91	1.10	1.14	1.19	1.15
C180×2.0-7.5	0.87	0.78	0.91	1.13	1.19	1.14
C180×2.2-7.5	0.96	0.89	1.06	1.26	1.34	1.28
C180×2.5-7.5	1.08	1.06	1.28	1.45	1.55	1.48
C200×2.0-7.5	0.92	0.82	1.07	1.27	1.35	1.29
C200×2.2-7.5	1.02	0.94	1.17	1.41	1.52	1.46
C200×2.5-7.5	1.15	1.13	1.41	1.61	1.76	1.69
C220×2.0-7.5	1.03	0.90	1.16	1.38	1.54	1.51
C220×2.2-7.5	1.14	1.05	1.31	1.54	1.71	1.74
C220×2.5-7.5	1.30	1.26	1.56	1.93	2.04	2.05
C250×2.0-7.5	1.04	0.96	1.30	1.56	1.79	1.82
C250×2.2-7.5	1.18	1.12	1.50	1.74	1.99	2.02
C250×2.5-7.5	1.40	1.35	1.80	2.01*	2.38	2.01
C220×2.0-9.0	0.74	0.66	0.80	0.98	1.07	1.01
C220×2.2-9.0	0.82	0.77	0.89	1.08	1.19	1.15
C220×2.5-9.0	0.92	0.92	1.11	1.26	1.38	1.35
C250×2.0-9.0	0.76	0.69	0.91	1.12	1.23	1.15
C250×2.2-9.0	0.87	0.81	1.04	1.23	1.38	1.33
C250×2.5-9.0	0.99	0.98	1.25	1.41	1.61	1.57
C280×2.5-9.0	1.07	1.00	1.38	1.57	1.83	1.78
C280×3.0-9.0	1.23	1.33	1.74	1.98	2.23	2.04
C300×2.5-9.0	1.15	1.11	1.52	1.86	2.08	2.06
C300×3.0-9.0	1.37	1.45	1.92	2.02*	2.57	2.06

and strength of corrugated steel sheet are the important factors to ensure the quality of mechanical occlusion.

3.6 Connection type

Table 7 shows that the ultimate bearing capacity of C purlins connected by self-drilling screws and standing seam clips respectively. Where, q_{uND} and q_{uNS} are the ultimate bearing capacity of purlins connected by self-drilling screws and standing seam clips, respectively. The ultimate bearing capacity of purlin-sheet roofs connected by standing seam clips is lower than that connected by self-drilling screws, except for C-1 purlins. For C-0 and C-2, the

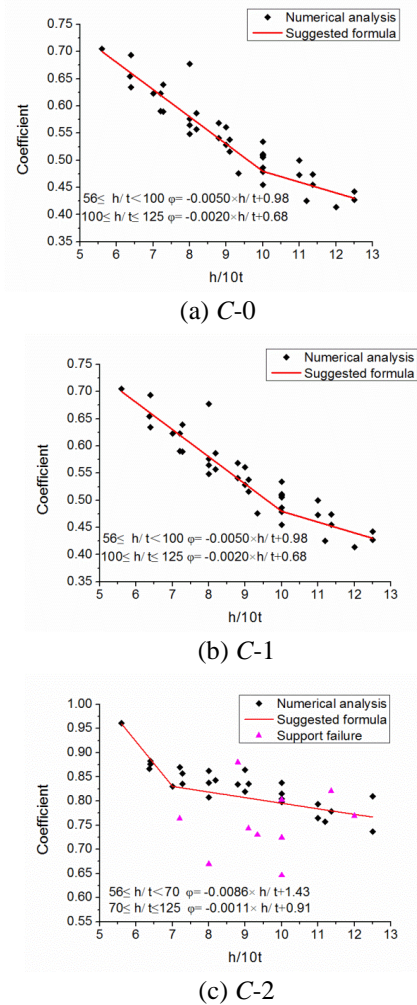


Fig. 11 Relationship between the coefficient ϕ and the height-thickness ratio of C purlins

ultimate bearing capacities of purlin-sheet roofs connected by standing seam clips are about 5.16% and 5.7% lower than that with self-drilling screws. For C-1, the ultimate bearing capacity of standing seam roof is 12.18% higher than the latter. This is because that the lateral displacement of C purlins can delay the distortional buckling of the lower flange in the middle span, while the lateral displacement of Z purlins can accelerate the distortional buckling of the lower flange. The variation laws of standing seam roofs are different from those connected by self-drilling screws.

4. Proposal of the design formulas

From the previous studies, the relationship between the ultimate bearing capacity and the uniaxial flexural capacity of C purlins are built through the coefficient ϕ . The coefficient ϕ is related to purlin type, number and position of anti-sag bars and depth-thickness ratio of purlin web. The relationship between the coefficient ϕ and the depth-thickness ratio of purlin web is shown in Fig. 11, based on the above analysis. Where, the red points mean failure of standing seam clips and the rest are the failure of purlins.

Considering that the expected failure modes are the failure of standing seam slips, the failure modes of support failure should be excluded.

When the thickness of corrugated steel sheet is larger than 0.6 mm, the proposed formulas for the coefficient of *C* purlins made by Q 235 is as follows.

For C-0 $56 \leq h/t < 100 \quad \varphi = -0.0050 \frac{h}{t} + 0.98 \quad (1)$

$100 \leq h/t < 125 \quad \varphi = -0.0020 \frac{h}{t} + 0.68 \quad (2)$

For C-1 $56 \leq h/t < 93 \quad \varphi = -0.0051 \frac{h}{t} + 1.19 \quad (3)$

$93 \leq h/t \leq 125 \quad \varphi = 0.71 \quad (4)$

$56 \leq h/t < 70 \quad \varphi = -0.0086 \frac{h}{t} + 1.43 \quad (5)$

For C-2 $70 \leq h/t \leq 125 \quad \varphi = -0.0011 \frac{h}{t} + 0.91 \quad (6)$

In some cases, the standing seam clips may fail ahead, while the purlins and sheets are well. Thus, it is common to see the failure of the roof under strong wind uplifts due to the failure of standing seam clips. From the previous analysis, the ultimate bearing capacity of the purlin-sheet roof lies between 2.00-2.06 kN/m. Then, the maximum load that the clips carried is 1.22 kN, where the spacing of clips is 612 mm. This load is lower than the ultimate bearing capacity shown in Table 2 and the standing seam clips are safe in the design.

The part presents the comparisons of several design formulas for the ultimate bearing capacity of purlins under wind suctions, including the proposed design formulas, Technical Code of Cold-Formed Thin-Wall Steel Structure (GB 50018 2002), and European Supplementary Provisions for Cold-Formed Components and Plates (EN 1993-1-3 2006).

In GB 50018-2002, the design formula is as follows.

$$\frac{M_x}{\varphi_b W_{ex}} + \frac{M_y}{W_{ey}} \leq f \quad (7)$$

In EN 1993-1-3 (2006), the design formulas for the lower flange is shown in Eq. (8).

$$\frac{1}{\chi_{LT}} \frac{M_{x,Ed}}{W_{eff,x}} + \frac{M_{y,Ed}}{W_{fy}} \leq f \quad (8)$$

Where, χ_{LT} is the reduction factor that can consider the effects of anti-sag bars. The design formulas for *C* purlins are shown in Eqs. (9)-(11).

C-0 $M_x \leq \frac{f}{\frac{1}{\chi W_{ex}} + \frac{\eta \cdot k}{W_{fy}}} \quad (9)$

C-0 $M_x \leq \frac{f}{\frac{1}{\chi W_{ex}} + \frac{\eta \cdot k}{4W_{fy}}} \quad (10)$

C-1 $M_x \leq \frac{f}{\frac{1}{\chi W_{ex}} + \frac{\eta \cdot k}{27W_{fy}}} \quad (11)$

The effective section modulus can be obtained according to the formulas for the effective section in

Table 8 Comparisons of predictions of ultimate bearing capacity of *C* purlins by different methods (kN·m)

Purlin type-span	C-0			C-1			C-2		
	M ₁	M ₂	M ₃	M ₁	M ₂	M ₃	M ₁	M ₂	M ₃
C140×2.0-6.0	3.26	1.13	3.06	4.31	3.16	2.24	4.31	3.78	2.86
C140×2.2-6.0	3.72	1.27	3.29	4.86	3.45	2.41	4.96	4.11	3.08
C140×2.5-6.0	4.39	1.50	3.60	5.67	3.88	2.64	5.95	4.59	3.39
C160×2.0-6.0	4.03	1.86	4.17	5.43	4.61	2.94	5.71	5.27	4.21
C160×2.2-6.0	4.66	2.07	4.51	6.20	5.03	3.18	6.28	5.74	4.56
C160×2.5-6.0	5.59	2.41	4.98	7.31	5.64	3.52	7.45	6.42	5.06
C180×2.0-6.0	4.76	2.94	5.29	6.56	6.30	3.71	7.28	6.99	5.79
C180×2.2-6.0	5.59	3.26	5.77	7.57	6.87	4.04	8.03	7.62	6.29
C180×2.5-6.0	6.80	3.74	6.43	9.03	7.71	4.50	9.12	8.53	7.01
C200×2.0-6.0	4.96	3.19	5.81	7.34	7.21	4.16	8.27	8.03	6.70
C200×2.2-6.0	5.93	3.52	6.34	8.19	7.86	4.53	9.13	8.75	7.28
C200×2.5-6.0	7.34	4.04	7.07	9.89	8.82	5.05	10.40	9.81	8.13
C160×2.0-7.5	4.03	1.29	4.26	5.43	3.96	3.15	5.71	4.94	3.84
C160×2.2-7.5	4.66	1.45	4.61	6.20	4.34	3.40	6.28	5.38	4.15
C160×2.5-7.5	5.59	1.71	5.10	7.31	4.90	3.76	7.45	6.03	4.58
C180×2.0-7.5	4.76	1.99	5.55	6.56	5.60	3.90	7.28	6.64	5.29
C180×2.2-7.5	5.59	2.22	6.04	7.57	6.12	4.25	8.03	7.24	5.74
C180×2.5-7.5	6.80	2.59	6.72	9.03	6.89	4.74	9.12	8.12	6.38
C200×2.0-7.5	4.96	2.15	6.12	7.34	6.37	4.29	8.27	7.62	6.07
C200×2.2-7.5	5.93	2.39	6.67	8.19	6.96	4.68	9.13	8.31	6.59
C200×2.5-7.5	7.34	2.78	7.44	9.89	7.84	5.22	10.40	9.32	7.33
C220×2.0-7.5	5.64	2.73	7.09	8.71	7.82	4.94	9.68	9.18	7.44
C220×2.2-7.5	6.43	3.03	7.76	9.51	8.54	5.40	10.71	10.02	8.09
C220×2.5-7.5	8.12	3.49	8.69	11.14	9.60	6.05	12.23	11.24	9.03
C250×2.0-7.5	6.23	2.99	7.85	10.29	9.12	5.56	11.20	10.80	8.79
C250×2.2-7.5	7.18	3.33	8.64	11.27	9.99	6.11	12.46	11.83	9.60
C250×2.5-7.5	8.59	3.85	9.75	12.71	11.28	6.88	14.32	13.34	10.79
C220×2.0-9.0	5.64	1.99	7.25	8.71	6.75	5.16	9.68	8.66	6.79
C220×2.2-9.0	6.43	2.22	7.92	9.51	7.39	5.65	10.71	9.45	7.39
C220×2.5-9.0	8.12	2.59	8.87	11.14	8.35	6.33	12.23	10.61	8.24
C250×2.0-9.0	6.23	2.17	8.04	10.29	7.79	5.70	11.20	10.16	7.90
C250×2.2-9.0	7.18	2.43	8.84	11.27	8.55	6.27	12.46	11.13	8.63
C250×2.5-9.0	8.59	2.83	9.97	12.71	9.70	7.07	14.32	12.55	9.69
C280×2.5-9.0	9.95	3.31	11.60	15.50	11.78	8.28	17.18	15.32	12.04
C280×3.0-9.0	13.32	4.15	13.65	18.43	14.13	9.76	20.95	18.22	14.19
C300×2.5-9.0	10.95	4.05	13.10	17.67	14.13	9.32	19.36	17.82	14.28
C300×3.0-9.0	14.21	5.05	15.51	21.02	16.90	11.04	23.68	21.20	16.88

previous reference (AISI S100 2007). Table 8 shows the calculation results of the design formulas in different codes/methods. Where, M1, M2, and M3 are the calculation results of the proposed formulas, GB50018-2002, and EN 1993-1-3: 2006. The predictions of *C*-0 purlins in GB50018 are conservative, only 42% of those by the proposed design formulas. For *C*-1 and *C*-2 purlins, the calculation results of GB50018 is a little lower than the proposed design formulas, about 82% and 90% of the proposed design formulas. This is because that the GB 50018-2002 does not consider the restraint of corrugated steel sheets on the purlins. For *C*-0 purlins, the calculation results of EN 1993-1-3 are consistent with those of the proposed design

formulas. For C-1 and C-2 purlins, the calculation results of EN 1993-1-3 are only 53% and 69% of those of the proposed design formulas. This is because for the purlins without anti-sag bars (C-0), the EN 1993-1-3: 2006 can take into account the effects of corrugated steel sheets and anti-sag bars.

However, for purlins with anti-sag bars (C-1 and C-2), the EN 1993-1-3: 2006 only considers the restraint of anti-sag bars and ignores the restraint of corrugated steel sheets. As mentioned above, the numerical calculations show that the diaphragm effect of corrugated steel sheet is significant, so the EN 1993-1-3: 2006 always underestimate the ultimate bearing capacity of the purlins with anti-sag bars. From above, the differences between the predictions of the proposed design formulas and GB 50018-2002 are significant. Relatively, the calculations of the proposed design formulas are consistent with those of EN 1993-1-3: 2006.

5. Conclusions

This paper presents parametric studies on the ultimate bearing capacities of purlin-sheet roofs connected by standing seam clips. In purlin-sheet roofs connected by standing seam clips, the failure modes and ultimate bearing capacity of C purlins are significantly different from those of Z purlins. It is always beneficial for setting the anti-sag bars near the lower flange, for the C purlin-sheet roofs. This is because it can reduce lateral displacement and torsional displacement, and improve the ultimate bearing capacity of purlins significantly. The ultimate bearing capacity of purlins increases slightly with sheet thickness increasing 0.6mm to 0.8mm.

The proposed formulas are simple and reliable. For purlins without anti-sag bars, the predictions of C-0 purlins in GB50018 are conservative, only 42% of those of the proposed design formulas, while the calculation results of EN 1993-1-3: 2006 are consistent with those of the proposed design formulas. This is because for purlins without anti-sag bars, GB 50018 does not consider the restraint of corrugated steel sheets on purlins, while EN 1993-1-3 can consider the restraint effects of sheet and anti-sag bars. For purlins with anti-sag bars (C-1 and C-2), the calculation results of GB50018 are a little lower than the proposed design formulas, while the EN 1993-1-3: 2006 underestimate the ultimate bearing capacity of purlins with anti-sag bars significantly. This is because for purlins with anti-sag bars, EN 1993-1-3 does not consider the restraint effect of corrugated steel sheets on purlins. From above, the differences between the calculations of the proposed design formulas and GB 50018-2002 are significant. Relatively, the predictions of the proposed design formulas are consistent with those of EN 1993-1-3: 2006.

Acknowledgments

The research described in this paper was financially supported by the Fundamental Research Funds for the Central Universities (Grant No. 2015QNA57).

References

- AISI S100 (2007), *North American specification for the design of cold-formed steel structural members*, American Iron and Steel Institute, Washington DC.
- Ali, H.M. and Senseny, P.E. (2003), "Models for standing seam roofs", *J. Wind Eng. Ind. Aerod.*, **91**, 1689-1702.
- Cai, J.G, Jiang, C., Deng, X.W., Feng, J. and Xu, Y.X. (2015), "Static analysis of a radially retractable hybrid grid shell in the closed position", *Steel Compos. Struct.*, **18**(6), 1391-1404.
- Cai, J.G., Ma, R.J., Deng, X.W. and Feng, J. (2016), "Static behavior of deployable cable-strut structures", *J. Constr. Steel Res.*, **119**, 63-75.
- Cai, J.G., Xu, Y.X., Feng, J. and Zhang, J. (2012), "In-plane elastic buckling of shallow parabolic arches under an external load and temperature changes", *J. Struct. Eng.*, ASCE, **138**(11), 1300-1309.
- Cai, J.G., Zhou, Y., Xu, Y.X. and Feng, J. (2013), "Non-linear stability analysis of a hybrid barrel vault roof", *Steel Compos. Struct.*, **14**(6), 571-586.
- El Damatty, A.A., Rahman, M. and Ragheb, O. (2003), "Component testing and finite element modeling of standing seam roofs", *Thin Wall. Struct.*, **41**, 1053-1072.
- European Committee for Standardization. EN 1993-1-3 (2006), *General rules-Supplementary rules for cold-formed members and sheeting*, British Standards Institution, London.
- Farquhar, S., Kopp, G. and Surry, D. (2005), "Wind tunnel and uniform pressure tests of a standing seam metal roof model", *J. Struct. Eng.*, ASCE, **131**(4), 650-659.
- GB 50017 (2003), *Code for Design of steel structure*, China Planning Press, Beijing.
- GB 50018 (2002), *Technical codes of cold-formed thin-wall steel structures*, China Planning Press, Beijing.
- Habte, F., Moonoghi, M.A., Chowdhury, A.G. and Irwin, P. (2015), "Full-scale testing to evaluate the performance of standing seam metal roofs under simulated wind loading", *Eng. Struct.*, **105**, 231-248.
- Johnston, N. and Hancock, G. (1994), "Calibration of the AISI R-factor design approach for purlins using Australian test data", *Eng. Struct.*, **16**, 342-347.
- Kachichian, M. and Dunai, L. (2012), "Purlin-cladding interaction in standing seam roofs", *Period Polytech. Civil Eng.*, **56**(1), 13-23.
- Katnam, K.B., Impe, V.R., Lagae, G. and Strycker, M.D. (2007), "A theoretical numerical study of the rotational restraint in cold-formed steel single skin purlin-sheeting systems", *Comput. Struct.*, **85**, 1185-1193.
- Liu, Y.X., Tong, G.S., Du, H.L. and Zhang, L. (2004), "Test and finite element analysis on torsional restraint of corrugated steel sheet to purlin through clips", *J. Build. Struct.*, **35**, 116-124.
- Lucas, R.M., Al-Bermani, F.G.A. and Kitipornchai, S. (1997), "Modelling of cold-formed purlin-sheeting system- part 2: simplified model", *Thin Wall. Struct.*, **27**, 263-286.
- Mahaarachchi, D. and Mahendran, M. (2009), "Wind uplift strength of trapezoidal steel cladding with closely spaced ribs", *J. Wind Eng. Ind. Aerod.*, **97**, 140-150.
- Morrison, M.J. and Kopp, G.A. (2012), "Analysis of wind-induced clip loads on standing seam metal roofs", *J. Struct. Eng.*, ASCE, **136**(3), 334-337.
- Prevatt, D.O., Schiff, S. D. and Sparks, P.R. (1995), "A technique to assess wind uplift performance of standing seam metal roofs", *Proceedings of the 11th Conference on Roofing Technology*, National Roofing Contractors Association, Gaithersburg, Maryland.
- Rousch, C.J. and Hancock, G.J. (1997), "Comparison of tests of bridged and unbridged purlins with a non-linear analysis model", *J. Constr. Steel Res.*, **41**, 197-220.

- Schafer, B.W. and Pekoz, T. (1999), "Laterally braced cold-formed steel flexural members with edge stiffened flanges", *J. Struct. Eng.*, ASCE, **125**, 118-127.
- Schroter, R.C (1985), "Air pressure testing of sheet metal roofing", *Proceedings of the 1985 International Symposium on Roof Technology, Structures and Techniques*, Chicago, Illinois.
- Serrette, R. and Pekoz, T. (1997), "Bending strength of standing seam roof panels", *Thin Wall. Struct.*, **27**, 55-64.
- Shoemaker, W.L. (2009), "Design and specification of standing seam roof panels and systems", *Proceedings of Structures 2009 Congress. Austin, Texas: Structural Engineering Institute of the American Society of Civil Engineers*, 726-735.
- Song, X.G. (2012), *Ultimate bearing capacity of cold-formed purlin-sheet roof under wind suctions*, Tongji University, Shanghai.
- Surry, D., Sinno, R., Nail, B., Ho, T., Farquhar, S. and Kopp, G. (2007), "Structurally effective static wind loads for roof panels", *J. Struct. Eng.*, ASCE, **133**(6), 871-885.
- Vrany, T. (2006), "Effect of loading on the rotational restraint of cold-formed purlins", *Thin Wall. Struct.*, **44**, 1287-1292.
- Zhang, L. and Tong, G.S. (2016), "Lateral buckling of simply supported C- and Z-section purlins with top flange horizontally restrained", *Thin Wall. Struct.*, **99**, 155-167.